

ROBUST ILC DESIGN USING MÖBIUS TRANSFORMATIONS

C. T. Freeman, P. L. Lewin and E. Rogers

University of Southampton

School of Electronics and Computer Science, University Road, Southampton, SO17 1BJ, United Kingdom

Keywords: Learning control, non-minimum phase systems, optimisation.

Abstract: In this paper a general ILC algorithm is examined and it is found that the filters involved can be selected to satisfy frequency-wise uncertainty limits on the plant model. The probability of the plant model being at a given point in the uncertainty space is specified, and the filters are then chosen to maximise the convergence rate that can be expected in practice. The magnitude of the change in input over successive trials and the residual error have also been incorporated into the cost function. Experimental results are presented using a non-minimum phase test facility to show the effectiveness of the design method.

1 INTRODUCTION

Iterative Learning Control (ILC) is a control method that is applicable to systems which perform the same action repeatedly. Operating in this way it is able to use past control information such as input signals and tracking errors in the construction of the present control action. This sets ILC apart from most other control techniques and has allowed it to provide improved performance with reduced knowledge of the plant when compared with other control approaches. A literature survey of ILC can be found in (Moore, 1998) and there exist textbooks on the subject (Moore, 1993; Bien and Xu, 1998). One such ILC update law is given by

$$u_{k+1} = F(z)u_k + S(z)e_k \quad (1)$$

where $e_k = y_d - y_k$ and $F(z)$ and $S(z)$ are filters which may be non-causal. This has been analysed in the frequency-domain in, for example, (Norrlöf and Gunnarsson, 1999) and (Norrlöf, 2000). Conversion of (1) to the frequency-domain using the sampling period, T_s , gives

$$U_{k+1} = F(e^{j\omega T_s})U_k + S(e^{j\omega T_s})E_k \quad (2)$$

Let the uncertain plant be described by $G(e^{j\omega T_s}) = G_0(e^{j\omega T_s})U(e^{j\omega T_s})$ where $U(e^{j\omega T_s})$ is a multiplicative uncertainty and G_0 the nominal plant model. In

this case the error evolution is

$$E_{k+1} = (F(e^{j\omega T_s}) - S(e^{j\omega T_s})G_0(e^{j\omega T_s})U(e^{j\omega T_s})) E_k + (1 - F(e^{j\omega T_s})) Y_d \quad (3)$$

so that

$$|F(e^{j\omega T_s}) - S(e^{j\omega T_s})G_0(e^{j\omega T_s})U(e^{j\omega T_s})| < 1 \quad (4)$$

is a necessary condition for stability since, for each frequency, (3) represents a state-space system in the iteration domain having a state transition matrix with eigenvalues less than 1. In particular, if $F(e^{j\omega T_s}) = 1$ this becomes a necessary condition for monotonic convergence which can be shown to be essentially a sufficient condition as well (Longman, 2000). More generally, the same argument means

$$|F(e^{j\omega T_s}) - S(e^{j\omega T_s})G_0(e^{j\omega T_s})U(e^{j\omega T_s})| < l \quad (5)$$

is a sufficient condition for the eigenvalues of the state transition matrix to be less than l , or a reduction of $\frac{1}{l}$ in the magnitude of the error over consecutive cycles if $F(e^{j\omega T_s}) = 1$. To accommodate both these cases, satisfying (5) will be said to produce a convergence rate of $\frac{1}{l}$.

Remark 1 Adding a filter, $T(z)$, on the $(k+1)^{th}$ cycle error to the algorithm given in (1) produces

$$u_{k+1} = F(z)u_k + S(z)e_k + T(z)e_{k+1} \quad (6)$$

and we can then write

$$y_{k+1} = \frac{G(z)T(z)}{1+G(z)T(z)}y_d + \frac{G(z)}{1+G(z)T(z)}(F(z)u_k + S(z)e_k) \quad (7)$$

to give

$$u_{k+1} = \frac{T(z)}{1+G(z)T(z)}y_d + \frac{1}{1+G(z)T(z)}(F(z)u_k + S(z)e_k) \quad (8)$$

The substitutions $\hat{y}_d = \left(\frac{T(z)}{S(z)} + 1\right)y_d$ and $\hat{G}(z) = \frac{G(z)}{1+G(z)T(z)}$, or alternatively $\hat{y}_d = \left(\frac{1}{S(z)} + \frac{1}{T(z)}\right)y_d$ and $\hat{G}(z) = \frac{G(z)T(z)}{1+G(z)T(z)}$, allow this to be written as (1). Any design method for $S(z)$ and $F(z)$ can therefore be implemented as (6) using these substitutions. Any robustness properties, however, will only apply to $\hat{G}(z)$ instead of $G(z)$.

2 DFT

An alternative expression for (2) is found by taking the Discrete Fourier Transform (DFT) of both sides of the update law (1) which results in

$$\hat{u}_{k+1} = \hat{F} \odot \hat{u}_k + \hat{S} \odot \hat{e}_k \quad (9)$$

which is possible since e_k and u_k are known prior to the $k + 1^{\text{th}}$ trial. Here \odot denotes component-wise multiplication and \hat{u} is the DFT of u . Similarly, the DFT of (3) results in an alternative description

$$\hat{e}_{k+1} = (\hat{F} - \hat{G}_0 \odot \hat{U} \odot \hat{S}) \odot \hat{e}_k + (I - \hat{F}) \odot \hat{y}_d \quad (10)$$

Note that now the design is conducted in the frequency-domain, the designer can select each element \hat{S}_i and \hat{F}_i individually and build the new input u_{k+1} using (9) combined with expressions for the DFT and IDFT of a signal. Similar transparency cannot be found in the time domain. Since (4) is a steady-state requirement which assumes a reasonable transient response, the use of a steady-state update of the input is not disadvantageous. It just remains to choose the value of the filters S and F at every frequency.

3 APPROACH TO FILTER DESIGN

By introducing the variable $v = U(e^{j\omega T_s})$ it is possible to write (5) as

$$\sup_{\omega \in [0, 2\pi]} |f(v)| < l \quad (11)$$

where

$$f(v) = F(e^{j\omega T_s}) - S(e^{j\omega T_s})G_0(e^{j\omega T_s})v \quad v \in \mathbb{C} \quad (12)$$

Let the open disc of radius l centred at the origin, and its boundary be defined as

$$\begin{aligned} D &= \{re^{j\theta} \mid \theta \in [-\pi, \pi], r \in [0, l]\}, \\ \delta D &= \{le^{j\theta} \mid \theta \in [-\pi, \pi]\} \end{aligned} \quad (13)$$

so that the inverse function

$$f^{-1}(v) = \frac{F(e^{j\omega T_s}) + v}{S(e^{j\omega T_s})G_0(e^{j\omega T_s})} \quad v \in \mathbb{C} \quad (14)$$

applied to D gives the range of values taken by $U(e^{j\omega T_s})$ for (5) to be satisfied.

The domain and co-domain can be enlarged to equal the extended complex plane $\hat{\mathbb{C}}$ (Jones and Singerman, 2004) which is the union of \mathbb{C} and the point at infinity; thus $\hat{\mathbb{C}} = \mathbb{C} \cup \{\infty\}$. In this case $f^{-1}(v)$ is an extended Möbius transformation when ω and T_s are fixed, and maps

- $\hat{\mathbb{C}}$ one-one onto $\hat{\mathbb{C}}$
- generalised circles onto generalised circles

A generalised circle is defined as either a circle or an extended line (see (Jones and Singerman, 2004) for details).

It is therefore possible to apply $f^{-1}(v)$ to δD and find the boundary of the region $U(e^{j\omega T_s})$ must occupy to ensure a convergence rate of $\frac{1}{l}$, or monotonic convergence if $l \leq 1$. The image of a Möbius transformation can be found by simply applying $f^{-1}(v)$ to three points of δD and finding the unique generalised circle which passes through the resulting points (see (Jones and Singerman, 2004)). Since $\{\pm l, lj\} \in \delta D$,

$$\begin{aligned} f^{-1}(+l) &= \frac{F(e^{j\omega T_s}) + l}{S(e^{j\omega T_s})G_0(e^{j\omega T_s})} \\ f^{-1}(-l) &= \frac{F(e^{j\omega T_s}) - l}{S(e^{j\omega T_s})G_0(e^{j\omega T_s})} \\ f^{-1}(lj) &= \frac{F(e^{j\omega T_s}) + lj}{S(e^{j\omega T_s})G_0(e^{j\omega T_s})} \end{aligned} \quad (15)$$

belong to this extended circle. However a simpler method involves noting that the inverse points of δD are 0 and ∞ so that the inverse points of the image are given by

$$f^{-1}(0) = \frac{F(e^{j\omega T_s})}{S(e^{j\omega T_s})G_0(e^{j\omega T_s})}, \quad f^{-1}(\infty) = \infty \quad (16)$$

and the mapping has the form

$$\left| z - \frac{F(e^{j\omega T_s})}{S(e^{j\omega T_s})G_0(e^{j\omega T_s})} \right| = k(e^{j\omega T_s}) \quad (17)$$

Since $f^{-1}(l) = \frac{F(e^{j\omega T_s}) + l}{S(e^{j\omega T_s})G_0(e^{j\omega T_s})} \in \delta D$ then

$$\begin{aligned} \left| \frac{F(e^{j\omega T_s}) + l}{S(e^{j\omega T_s})G_0(e^{j\omega T_s})} - \frac{F(e^{j\omega T_s})}{S(e^{j\omega T_s})G_0(e^{j\omega T_s})} \right| \\ = k(e^{j\omega T_s}) = \frac{l}{|S(e^{j\omega T_s})G_0(e^{j\omega T_s})|} \end{aligned} \quad (18)$$

which is the equation for a circle with centre, λ , and radius, r , where

$$\lambda = \frac{F(e^{j\omega T_s})}{S(e^{j\omega T_s})G_0(e^{j\omega T_s})}, \quad r = \frac{l}{|S(e^{j\omega T_s})G_0(e^{j\omega T_s})|} \quad (19)$$

This circle can then be drawn for every frequency of interest and hence the region $U(e^{j\omega T_s})$ must occupy in order to guarantee monotonic convergence. Note that a Möbius transformation, $t(z)$, maps a region R in its domain to a region $t(R)$, and the boundary of R to the boundary of $t(R)$. Figure 1 shows the action of $f^{-1}(v)$ on δD and the region $U(e^{j\omega T_s})$ must occupy for a convergence rate of $\frac{1}{l}$. Any uncertainty

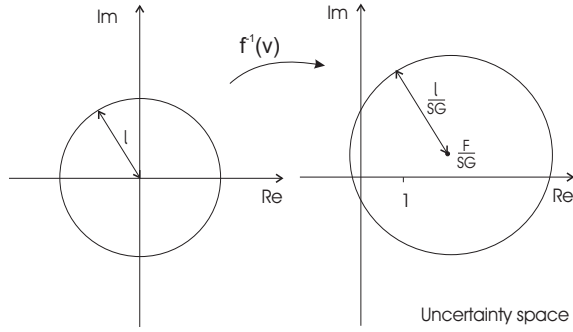


Figure 1: Geometry of uncertainty space

that is contained within the right-hand circle for all frequencies will satisfy (5). At a general point, p , in the uncertainty space we can equate the distance from p to λ with r

$$\left| p - \frac{F(e^{j\omega T_s})}{S(e^{j\omega T_s})G_0(e^{j\omega T_s})} \right| = \frac{l}{|S(e^{j\omega T_s})G_0(e^{j\omega T_s})|} \quad (20)$$

in order to find the convergence rate at that frequency

$$\begin{aligned} \frac{1}{l} &= \frac{1}{\left| p - \frac{F(e^{j\omega T_s})}{S(e^{j\omega T_s})G_0(e^{j\omega T_s})} \right| |S(e^{j\omega T_s})G_0(e^{j\omega T_s})|} \\ &= \frac{1}{|S(e^{j\omega T_s})G_0(e^{j\omega T_s})p - F(e^{j\omega T_s})|} \end{aligned} \quad (21)$$

This provides a useful means of selecting S and F : Let us choose to maximize the convergence rate that can be expected given that the probability that the plant is at the point p at a given frequency is known or can be estimated. It will be assumed that this probability is symmetrical about the nominal value, that is $+1$ in the uncertainty space. This is a situation which is realistic given the methods of obtaining a plant model commonly used in practice. In this case it will be a function of the distance to the nominal plant model which equals $\frac{1}{|p-1|}$ in the uncertainty space. The optimisation will therefore take the form

$$\max_{S,F} J(S,F) \quad (22)$$

with the cost function

$$\begin{aligned} J(S,F) &= \int_A \frac{1}{\left| p - \frac{F}{SG_0} \right| |SG_0|} P\left(\frac{1}{|p-1|}\right) \delta p \\ &= \frac{1}{|SG_0|} \int_A \frac{1}{\left| p - \frac{F}{SG_0} \right|} P\left(\frac{1}{|p-1|}\right) \delta p \end{aligned} \quad (23)$$

where $P(\cdot)$ is the probability that the plant is at p , and A is a region of uncertainty over which $P(\cdot)$ is valid. The frequency dependence of the filters has been dropped for conciseness. Note that a small circle around the singularity must be removed if the equation is solved numerically. Figure 2 shows three cases using the probability function $P(x) = x^{-\alpha}$ and α equal to 2, 1 and 0.5. The probability function is able

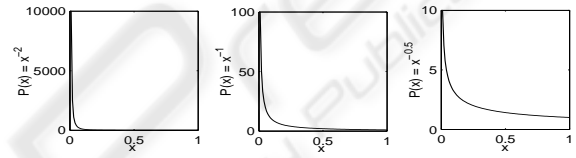


Figure 2: Examples of $P(x)$

to shift focus between robustness and convergence speed by varying the weighting of the optimisation. In the first case $P(x)$ is only large for $x \approx 0$ so the maximisation will lead to a solution which is tailored to only values close to the nominal plant model. As α is reduced it becomes more important to choose S so that the whole of A has a value of $l < 1$. These cases are shown in Figure 3. In a) $\frac{1}{SG} \approx 1$ to give a high convergence rate for the nominal plant, whilst in b) it is smaller but most of the region A has the property of satisfying (5). This choice of $P(x)$ produces the cost

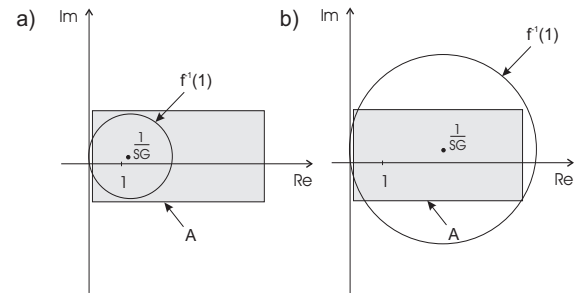


Figure 3: Optimal solutions for a) $\alpha > 1$ and b) $\alpha < 1$

$$J(S,F) = \frac{1}{|SG_0|} \int_A \frac{|p-1|^\alpha}{\left| p - \frac{F}{SG_0} \right|} \delta p \quad (24)$$

and the values of S and F are found by solving

$$\frac{\partial}{\partial S} J(S, F) = 0 \quad \text{and} \quad \frac{\partial}{\partial F} J(S, F) = 0 \quad (25)$$

at each frequency and ensuring that it is a global maximum. If F is fixed at 1 then any solution, S^* which solves (25), so that

$$\frac{dJ(S^*, 1)}{dS} = 0 \quad (26)$$

will also solve the optimisation using

$$J\left(\frac{S}{F}\right) = \frac{|F|}{|S||G_0|} \int_A \frac{|p-1|^\alpha}{\left|p - \frac{F}{SG_0}\right|} \delta p \quad (27)$$

since only a substitution of variables has been applied. S and F can assume any values as long as $\frac{S}{F} = S^*$. If F is now fixed at \hat{F} , the corresponding value of \hat{S} is $\hat{F}S^*$. This must also solve the optimisation using (24) as this is simply (27) multiplied by a constant. Therefore it is enough to solve the optimisation using (24) with $F = 1$ and simply substitute $\hat{S} = \hat{F}S^*$ to obtain the solution for every other value of F . The resulting cost is $\hat{J} = |\hat{F}|J^*$ where J^* is the cost using $F = 1$. In order to incorporate other considerations in the cost, let us consider the change in input from one trial to the next. Since this is given by

$$u_{k+1} - u_k = (F - 1)u_k + Se_k \quad (28)$$

which, with the repeated application of (3), becomes

$$u_{k+1} - u_k = S(F - SG_0U)^k e_0 + S(1 - F) \sum_{i=0}^{k-1} (F - SG_0U)^i y_d + (F - 1)u_k \quad (29)$$

and the residual error is given by

$$e_k = (F - SG_0U)^k e_0 + (1 - F) \sum_{i=0}^{k-1} (F - SG_0U)^i y_d \quad (30)$$

It can be seen that reducing F from 1 therefore has the effect of reducing the cost (24) with the compromise of a likelihood of increased residual error and input change. To tackle these effects directly for an arbitrary e_0 and y_d , it is required that each term in (29) and (30) has a small modulus for each frequency considered. Assuming that (4) is satisfied it remains to reduce $|S|$ and also the bound, λ , on the remaining term which is given by

$$(1 - F) \sum_{i=0}^{k-1} (F - SG_0U)^i y_d < \frac{1 - F}{1 - (F - SG_0U)} = \lambda \quad (31)$$

This can be achieved using the mapping technique that has already been described. Using this, we find

that at a point in the uncertainty space, p , the bound λ equals

$$\frac{1 - F}{SG_0 \left| p + \frac{1 - F}{SG_0} \right|} = \frac{1}{\left| \frac{SG_0}{1 - F} p + 1 \right|} \quad (32)$$

Therefore the functions $Q(|S|^{-1})$ and $R\left(\left|\frac{SG_0}{1 - F} p + 1\right|\right)$ can be incorporated into the cost to limit the upper bound of the residual error and change in successive inputs. Since these are dependent on the plant and choice of y_d , they will be neglected in order to maintain focus on the general case.

3.1 Experimental Test Facility

The experimental non-minimum phase test-bed has previously been used to evaluate a number of Repetitive Control and ILC schemes (see (Freeman et al., 2005) for details) and consists of a rotary mechanical system of inertias, dampers, torsional springs, a timing belt, pulleys and gears. An encoder records the output shaft position and a standard squirrel cage induction motor drives the load. The system has been modelled using a LMS algorithm to fit a linear model to a great number of frequency response test results. The resulting continuous time plant transfer function has thus been established as

$$G_0(s) = \frac{1.202(4 - s)}{s(s + 9)(s^2 + 12s + 56.25)} \quad (33)$$

A PID loop around the plant is used in order to act as a pre-stabiliser and provide greater stability. The PID gains used are $K_p = 137$, $K_i = 5$ and $K_d = 3$. The resulting closed-loop system constitutes the system to be controlled.

4 EXPERIMENTAL RESULTS

In polar co-ordinates let us define the region

$$A = \{re^{j\theta} \mid \theta \in [\theta_m \ \theta_M], r \in [r_m \ r_M]\} \quad (34)$$

in the uncertainty space over which the probability function is valid. The parameters $T = 6$ and $n = 1024$ are chosen for convenience to give $f_s = 1024/6$. Let us solve the optimisation using (24) with $F = 1$ and $\alpha = 0.2$. Figure 4 shows a Bode plot of the resulting S vectors when using $\theta_m = -\frac{\pi}{6}$, $\theta_M = \frac{\pi}{6}$, $r_m = 0$ and $r_M = \frac{1 + \frac{T\omega}{2\pi\lambda}}{|G_0|^2}$ with $\lambda = 4, 6, 8, 10$. These have been chosen using previous experience of the plant uncertainty. As λ increases, r_M decreases, which, in turn, increases the magnitude of S at each frequency as the plant effectively becomes less uncertain as A diminishes in size. Since $\theta_m = -\theta_M$,

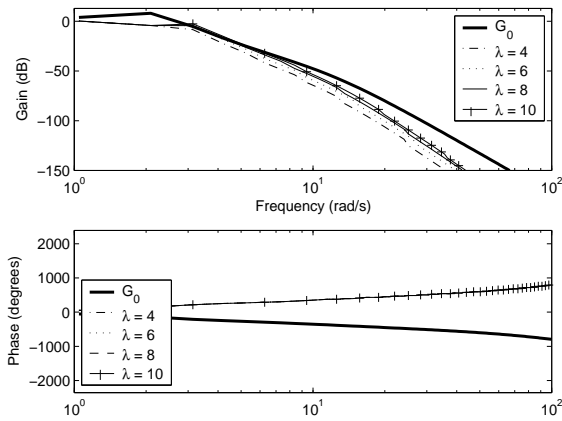


Figure 4: Bode plot using various r_M functions and $\alpha = 0.2$

A is symmetrical about the real axis which results in $\angle S = -\angle G_0$. Figure 5 shows error results using the sinewave demand (shown in figure 11). The normalized error ‘NE’ is the cumulative error incurred over an iteration divided by the integral of the reference demand. Data has been recorded over the course of 200 iterations. It can be seen that smaller λ values lead to reduced fluctuations in the cycle error. Figure 6 shows

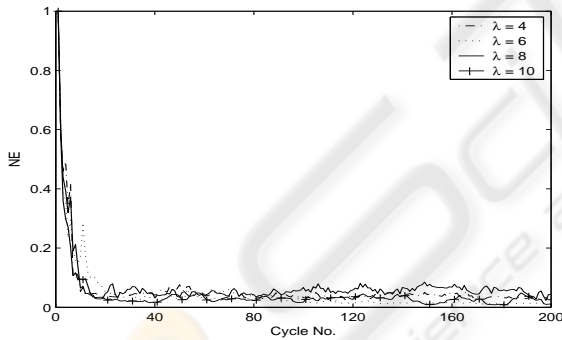


Figure 5: Cycle error for sinewave demand

error results using the sinewave demand (shown in figure 7). Due to the higher frequencies present in the demand, the convergence is slower and the residual error greater. Higher frequency properties of the optimisation play a greater role and so the effect of λ on the learning transients is more pronounced than previously. The convergence of the output to the demand is shown in figure 7 using $\lambda = 6$. The repeating sequence demand is also drawn.

To investigate the effect of variation in α , the optimisation using (24) with $F = 1$ has again been solved but using $\alpha = 0.1, 0.3, 0.5, 0.7$. Figure 8 shows a Bode plot of the resulting S vectors when

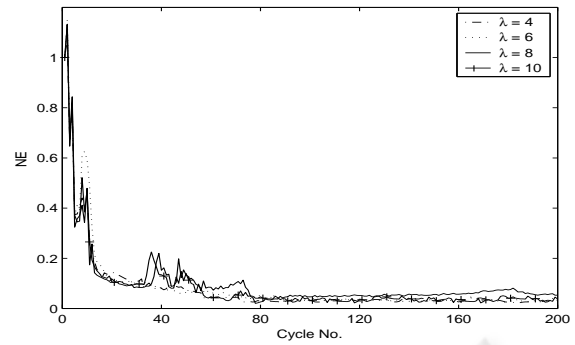


Figure 6: Cycle error for repeating sequence demand

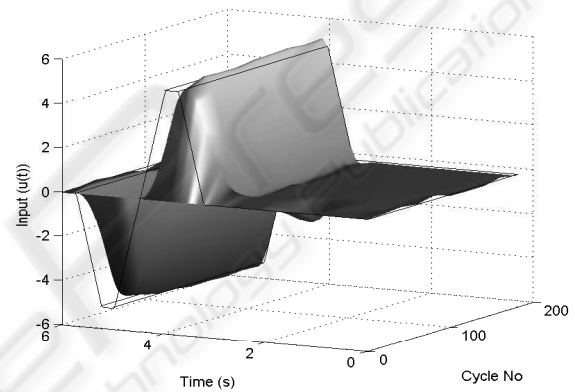


Figure 7: Output tracking using repeating sequence demand and $\lambda = 6$

using $\theta_m = -\frac{\pi}{6}$, $\theta_M = \frac{\pi}{6}$, $r_m = 0$ and $r_M = \frac{1 + \frac{T\omega}{2\pi\lambda}}{|G_0|^2}$ with $\lambda = 6$. As α increases in magnitude more emphasis is put on fast convergence for the nominal plant and the gain is larger for a greater range of frequencies. Figure 9 shows error results using the sinewave demand and it can be seen that higher α values produce greater learning transients, and, ultimately, divergence. They do, however, produce faster initial convergence. Figure 10 shows error results using the repeating sequence demand which confirm the previous findings. The convergence of the output to the demand is shown in figure 11 using $\alpha = -0.5$ and the sinewave demand which is also shown.

5 FUTURE WORK

Since the uncertainty probability function can only be an approximation, an obvious method to increase algorithm robustness is to use additional plant data and attempt to locate the plant model with greater accu-

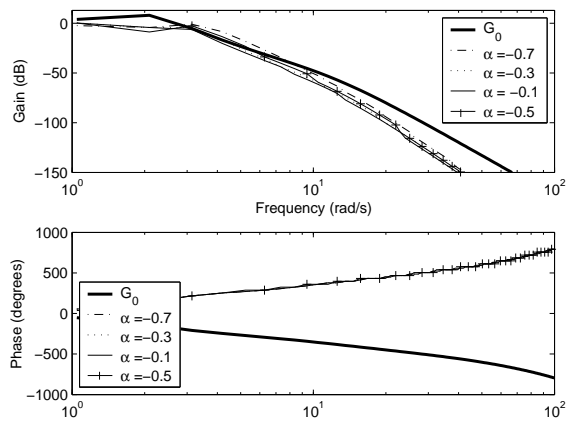


Figure 8: Bode plot using various α , $\lambda = 6$

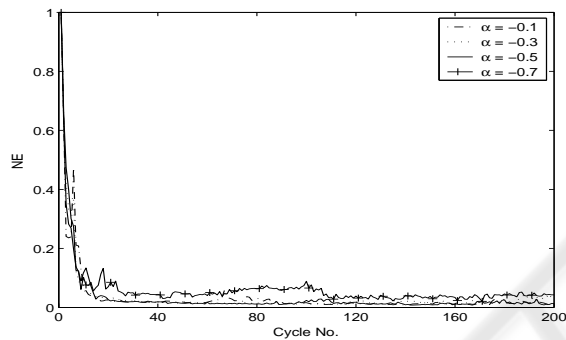


Figure 9: Cycle error for sinewave demand

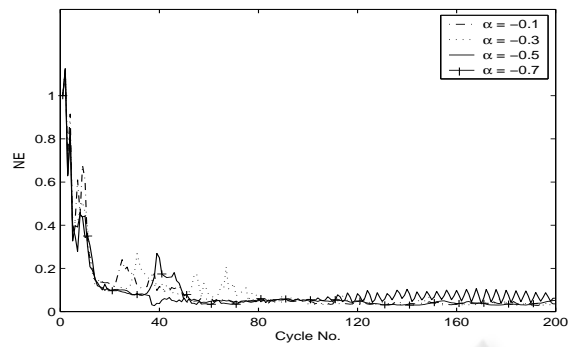


Figure 10: Cycle error for repeating sequence demand

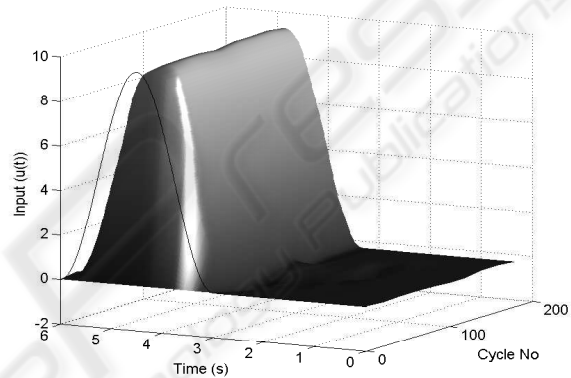


Figure 11: Output tracking using sinewave demand and $\alpha = 0.5$

racy as the iterations progress. At the same time, the added confidence in the nominal plant value could allow the focus of the optimisation to be shifted from robustness to convergence speed. This would be achieved by adaptively varying the probability function from trial to trial and seeking to reduce the radii of circles corresponding to convergence rates for each frequency around the nominal plant model. This use of adaptive parameter tuning will be investigated in conjunction with different plant models to confirm its effectiveness.

The terms that have been derived in order to tackle the magnitude of the residual error and the change in input over successive cycles must be added to the cost function and experiments conducted to examine their performance in practice.

REFERENCES

Bien, Z. and Xu, J. (1998). *Iterative Learning Control, Analysis, Design, Integration and Applications*. Kluwer Academic Publishers.

Freeman, C. T., Lewin, P. L., and Rogers, E. (2005). Experimental evaluation of iterative control algorithms for non-minimum phase plants. *International Journal of Control*, 78(11):806–826.

Jones, G. A. and Singerman, D. (2004). *Complex Functions: An Algebraic and Geometric Viewpoint*. Cambridge University Press.

Longman, R. W. (2000). Iterative learning control and repetitive control for engineering practice. *International Journal of Control*, 73(10):930–954.

Moore, K. L. (1993). *Iterative Learning Control for Deterministic Systems*. Springer-Verlag.

Moore, K. L. (1998). Iterative learning control - an expository overview. *Applied and Computational Controls, Signal Processing and Circuits*, 1(1):151 – 214.

Norrlöf, M. (2000). Comparative study on first and second order ilc- frequency domain analysis and experiments. In *Proceedings of the 39th Conference on Decision and Control*, pages 3415–3420.

Norrlöf, M. and Gunnarsson, S. (1999). A frequency domain analysis of a second order iterative learning control algorithm. In *Proceedings of the 38th Conference on Decision and Control*, pages 1587–1592.